Research in Astronomy and Astrophysics, 23:105009 (9pp), 2023 October https://doi.org/10.1088/1674-4527/acf031

The AGN Feedback in Compact Galaxies: On the Impact of a More Massive Central Black Hole

Yihuan Di[1,2], Feng Yuan[1,2], and Suoqing Ji[1]
[1] Shanghai Astronomical Observatory, Chinese Academy of Sciences, Shanghai 200030, China
[2] University of Chinese Academy of Sciences, Beijing 100049, China; fyuan@shao.ac.cn
Received 2023 May 22; revised 2023 July 13; accepted 2023 July 26; published 2023 September 20

Abstract

We conduct high-resolution hydrodynamical simulations using the MACER framework to investigate the interplay between the interstellar medium, active galactic nuclei (AGN) feedback and black hole (BH) feeding in a massive compact galaxy, with an emphasis on the impact of different central BH masses. We find that with a more massive central BH, high-speed outflows are more prominent, and the gas fraction in the compact galaxy is reduced. Due to the lower gas density and higher gas temperature, the compact galaxy with a more massive BH (`MAS` galaxy) remains predominantly single-phase with the cooling time $t_{\rm cool} \gtrsim 100 t_{\rm ff}$. In contrast, the compact galaxy with the reference BH mass (`REF` galaxy) maintains a higher gas fraction with a shorter cooling time, slightly more multiphase gas and less prominent outflows. We further demonstrate that the difference in gas thermal states and kinematics is caused by the stronger AGN feedback in the compact galaxy with a more massive BH, where the AGN wind power is twice as much as that with the reference BH. Since the AGN feedback efficiently suppresses the inflow rate and the BH feeding rate, the BH mass growth is significant in neither the compact galaxy with the reference BH nor that with the more massive BH, only by 24% and 11% of the initial BH mass, respectively, over the entire evolution time of 10 Gyr. We thus posit that without ex situ mass supply from mergers, the massive BHs in compact galaxies cannot grow significantly via gas accretion during the late phase, but might have already formed by the end of the rapid early phase of galaxy formation.

Key words: galaxies: active – galaxies: evolution – galaxies: nuclei – (galaxies:) quasars: supermassive black holes

1. Introduction

It is suggested by observations that most primeval massive galaxies at high redshifts of ∼2 are compact, characterized by relatively large stellar masses $\gtrsim 10^{11} M_{\odot}$, but small effective radii $\lesssim 2$ kpc (Daddi et al. 2005; Trujillo et al. 2006, 2007). However, most of the compact massive galaxies are absent from low redshifts, which invokes a puzzle of the fate of these objects. One plausible guess is that these compact massive galaxies have significantly expanded in size over time, and ultimately evolved into the present-day massive elliptical galaxies (van Dokkum et al. 2010), while the details of the evolution are still unclear. A *two phases* evolution model has been suggested by numerical simulations (Naab et al. 2009; Oser et al. 2010) which constitutes a rapid early phase at $z \gtrsim 2$ followed by an extended late phase at $z \lesssim 2$. In the early phase, stars in galaxies form in situ fueled by cold gas inflows, with a variety of mechanisms (e.g., disk instabilities and wet mergers) driving the gas to the galaxy center and sustaining the compact shape. In the late phase, after the cold gas is exhausted and the galaxies become quenched, their growth is dominated by the accretion of ex situ stars from dry mergers (Hopkins et al. 2009).

The majority of compact galaxies at high redshifts undergo the second phase of evolution. However, due to the stochastic nature of mergers, a small fraction of compact galaxies can bypass the second phase (Quilis & Trujillo 2013). These exceptional cases can be found in the local universe. The first confirmed example of a low-redshift compact massive galaxy, exhibiting small effective radii, massive stellar mass and an old stellar population, is NGC1277 in the Perseus cluster (Trujillo et al. 2013). More recently, Ferré-Mateu et al. (2017) confirmed the existence of two additional "red nuggets" in the present-day Universe: MRK 1216 and PGC 032 873. These galaxies possess stellar masses reaching approximately $2 \times 10^{11} M_{\odot}$, resulting in compact morphologies ($R_e \sim 2$ kpc) and an old stellar population (age exceeding 10 Gyr).

However, direct measurement of the mass of central black holes in compact galaxies is extremely challenging. As for now, observations have not yet converged on a consensus regarding the mass of the central black hole in these galaxies. For instance, estimates of the central black hole mass in the first discovered compact galaxy, NGC 1277, vary by orders of magnitude. van den Bosch et al. (2012) estimate its mass as $1.7 \times 10^{10} M_{\odot}$, which, if confirmed, would make it the most massive central black hole discovered thus far based on observational evidence. In contrast, Walsh et al. (2016) report a lower mass of $5 \times 10^9 M_\odot$ for this central black hole, still a considerable value. On the other hand, Graham et al. (2016) argue that the black hole's mass is $1.2 \times 10^9 M_\odot$, aligning with the latest $M_{\rm bh}$–$M_{\rm bulge}$ relationship.

Additionally, Ferré-Mateu et al. (2015) discovered that compact galaxies with old stellar populations possess more massive central black holes, which represent extreme outliers in the scaling relation between $M_{\rm bh}$ and their host galaxies. They propose a hypothesis that the central black hole formation occurs during the first phase of galaxy evolution and ceases after approximately 10 Gyr. According to semi-analytical models, if an individual galaxy expands its size by approximately seven times, it can increase its mass by nearly a factor of five. Considering the missing stellar mass, the mass of the black hole in compact galaxies would align even more closely with the scaling relations observed in the local universe.

Werner et al. (2018) concur that the central black hole can indeed grow through a process known as chaotic cold accretion (CCA; Gaspari et al. 2013). In this mechanism, multiphase gas condenses out of the hot halo and subsequently falls onto the center of the galaxy. Within a timescale of 10 Gyr, the central black hole in an isolated elliptical galaxy can grow to several $10^9 M_\odot$ with CCA and mechanical AGN feedback (Gaspari et al. 2018). However, in our previous study, we find that the central black hole mass in a compact galaxy only increased by several $10^8 M_\odot$, which is only approximately 50% higher than its initial mass. At present, the question of whether the mass growth of black holes at the center of compact galaxies is primarily due to initial galaxy formation during the first phase or accreted through subsequent evolution remains unclear.

The strengths of AGN feedback strongly depend on different factors, in particular, the masses of the central black holes, about which previous literature is relatively sparse. Yao et al. (2021) examine the influence of different black hole masses on AGN feedback in giant elliptical galaxies. They discover that smaller central black holes exhibit stronger oscillations in the black hole accretion rate and AGN luminosity, along with higher star formation rates. However, it is uncertain whether these findings apply to compact galaxies. Due to their deeper gravitational potential wells, compact galaxies accrete more interstellar medium (ISM) toward their centers. Besides, Yao et al. (2021) primarily focus on the impact of AGN feedback rather than its effect on galactic gas properties. We are thus motivated to investigate the gas properties of compact galaxies and examine how the mass of the supermassive black hole influences these properties.

This paper is structured as follows. In Section 2, we briefly introduce the framework of our models, including the galaxy set-ups, stellar feedback, star formation, and AGN feedback. In Section 3, we show our results. Finally, in Section 4, we summarize our results.

2. Methodology

We use a numerical setup similar to that in Di et al. (2023), and only briefly describe the main features here. Our simulations are performed using the MACER (Massive AGN Controlled Ellipticals Resolved) framework. This code is a high-resolution hydrodynamical numerical simulation based on the parallel ZEUS-MP code (Hayes et al. 2006). MACER adopts 2.5D axisymmetric spherical coordinates denoted by (r, θ, ϕ), where the axisymmetry is in the ϕ-direction. In the θ direction, the mesh is divided homogeneously into 30 grids (5°–175°); while in the radial direction, we use a logarithmic mesh covering the radial range of 0.8 pc $\sim$ 160 kpc. With such grids, the finest resolution is achieved at the innermost grid, which is $r_{\rm in} = 0.17$ pc. Our inner boundary is smaller than the Bondi radius of the black hole. In this case, once we calculate the mass flux at the inner boundary, we can safely combine it with the theory of black hole accretion to obtain the mass accretion rate of the black hole horizon and subsequently the outputs of AGN (see Yuan et al. (2018) for details).

To investigate the effect of black hole mass, in the present work, we simulate two galaxies with different black hole masses, as we will describe below. The initial conditions of the two galaxies are described in Section 2.1. Important physical processes in our simulations include AGN and stellar feedback, and radiative heating and cooling. For the calculation of radiative heating and cooling, we use the formula presented in Sazonov et al. (2005). The processes considered include Compton heating and cooling, bremsstrahlung loss, photoionization, and line and recombination heating and cooling. In Section 2.2, we describe how we model the AGN and stellar feedback.

2.1. Galaxy Initial Conditions

There are multiple definitions of Compact Massive Galaxies (de la Rosa et al. 2016). The restrictive compactness criterion we use is proposed by van Dokkum et al. (2015):

$$\log(R_{\rm e}/{\rm kpc}) \leqslant \log(M_\star/M_\odot) - 10.7 \quad (1)$$

with $\log(M_\star/M_\odot) \geqslant 10.6$. We check the TNG-100 data at $z = 2$ by this criterion and choose ID:58771 as the representative of compact massive galaxies.

The dark matter halo of this galaxy is described by an NFW (Navarro–Frenk–White) profile (Navarro et al. 1996). It is characterized by a scale radius of $r_{\rm s} = 8.268$ kpc and a dark matter mass of $M_{\rm DM} = 2.98 \times 10^{12} M_\odot$. To model the stellar component, a spherically symmetric Jaffe model (Dehnen 1993) is employed. It is characterized by an effective radius of $r_{\rm eff} = 1.03$ kpc and a stellar mass of $M_{\rm star} = 1.52 \times 10^{11} M_\odot$.

Here all the parameter values are obtained by fitting the TNG-project simulation data (TNG-100, $z = 2$, ID:58771). The initial gas is assumed to be negligibly rare. This assumption does not affect our simulation since the gas generated by the

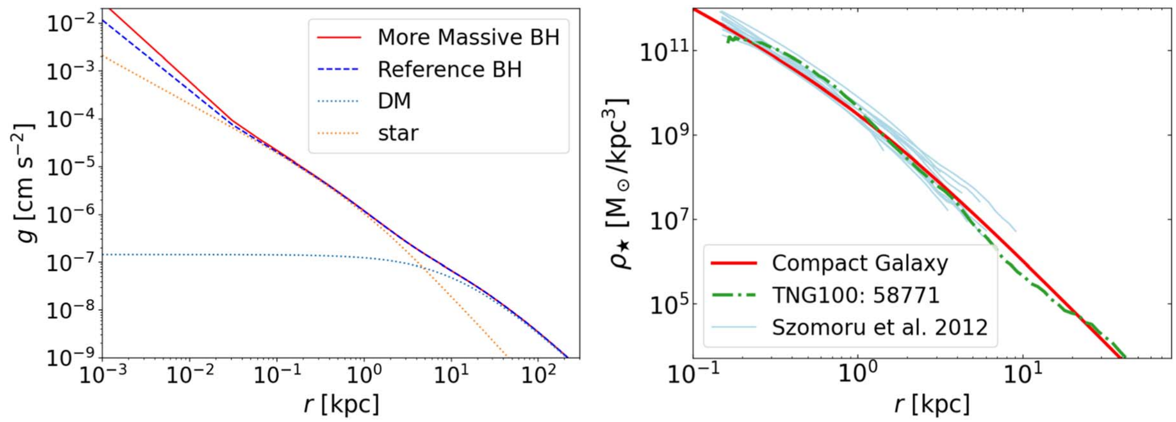

Figure 1. Left panel: the gravitational potential of the compact galaxies with reference BH and more massive BH. With 30 pc as the dividing line, a more massive black hole has a stronger gravitational force in it. Right panel: the stellar profile of the compact galaxies (red solid line) employed in this study. For comparison, the profiles of a selection of compact massive galaxies at $z \sim 2$ are also depicted with light blue lines (Szomoru et al. 2012). The green lines denote the original data sourced from IllustrisTNG.

star wind can fill the entire galaxy after the simulation starts. The initial masses of the black hole in the two galaxies are $M_{\rm BH} = 6.723 \times 10^8\,M_\odot$ (reference BH, the `REF` run) and $M_{\rm BH} = 1.8 \times 10^9\,M_\odot$ (more massive BH, the `MAS` run). The left panel of Figure 1 shows the gravitational potential of the compact galaxies with different BH masses. Within 30 pc their gravitational potential is different. The right panel of Figure 1 is the stellar profile of our simulation and some observation sample.

2.2. Physical Processes

2.2.1. AGN Feedback

Black hole accretion, and correspondingly AGN feedback, is divided into two modes depending on the mass accretion rate of the black hole. The boundary accretion rate can be inferred from the observations on the state transition of BH X-ray binaries, which is $L_{\rm c} \approx 2\% L_{\rm Edd}$ or $\dot{M}_{\rm c} \approx 2\% \dot{M}_{\rm Edd}$. We adopt this value for AGN since the physics of accretion is largely independent of black hole mass. Smaller than this rate, the black hole accretion and AGN feedback will be in the hot mode; while above this rate it is in the cold mode.

The cold and hot accretion modes are described by the standard thin disk (Shakura & Sunyaev 1973) and the hot accretion flows (Yuan & Narayan 2014), respectively. Both radiation and wind feedback are taken into account in each mode. For AGN wind, we treat it as a source term by adding the energy, momentum and mass of the wind into the innermost two grids of the simulation domain. For AGN radiation, in addition to heating/cooling, we also consider the radiation pressure to the gas.

During the cold accretion mode, the gas freely falls until a disk is formed at the circularization radius. The black hole accretion rate is determined by solving a set of differential equations. These equations take into account the accretion rate at the inner boundary, the mass evolution of the small disk and the mass lost through the wind. The bolometric luminosity is calculated by

$$L_{\rm BH} = \epsilon_{\rm cold} \dot{M}_{\rm BH} c^2 \tag{2}$$

The radiation efficiency is set to $\epsilon_{\rm cold} = 0.1$. In addition to luminosity, another parameter to describe the radiative heating to the ISM of the host galaxy by Compton scattering is the Compton temperature of the radiation. In the cold model, its value is $T_{\rm C} = 2 \times 10^7$ K (Sazonov et al. 2004).

Wind production in the cold mode is still a partially solved problem. Many mechanisms seem to play a role in producing wind, such as thermal, magnetic, and radiation. Therefore, we adopt the observational results of Gofford et al. (2015) to describe the wind properties. They analyzed a sample of 51 *Suzaku*-observed AGNs and measured the mass flux and velocity of the wind:

$$\dot{M}_{\rm W,C} = 0.28 \left(\frac{L_{\rm bol}}{10^{45}\ {\rm erg\ s^{-1}}} \right)^{0.85} M_\odot\ {\rm yr^{-1}}, \tag{3}$$

$$v_{\rm W,C} = 2.5 \times 10^4 \left(\frac{L_{\rm bol}}{10^{45}\ {\rm erg\ s^{-1}}} \right)^{0.4} {\rm km\ s^{-1}}. \tag{4}$$

We set the maximum wind velocity of $10^5\ {\rm km\ s^{-1}}$.

In contrast to the case of the cold mode, observational constrains on wind in the hot mode are still relatively poor (but see Shi et al. (2021)), but the theoretical study of wind is very mature (e.g., Yuan et al. 2012, 2015; Yang et al. 2021). In the 3D GRMHD simulation of Yuan et al. (2015), they have used the "virtual particle trajectory" approach and successfully

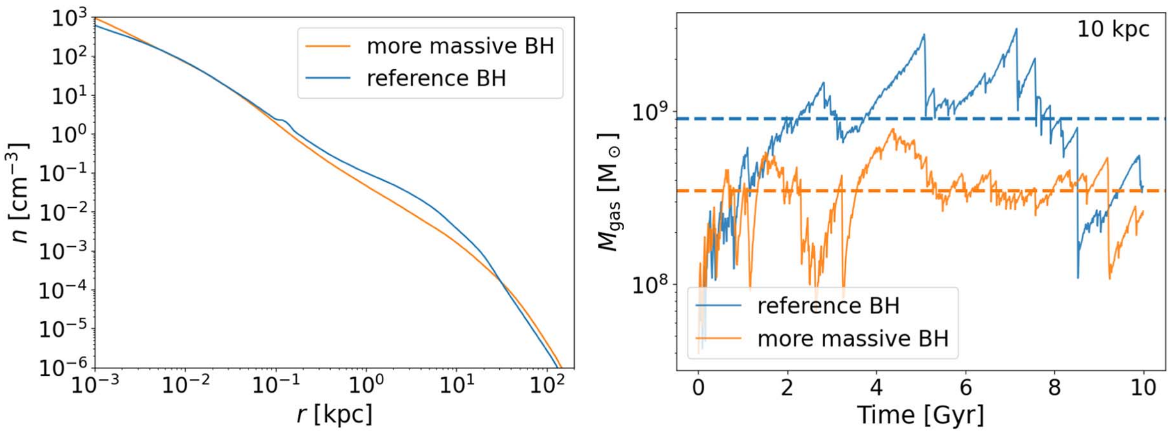

Figure 2. Left panel: the mean radial distribution of the gas number density during 10 Gyr. Reference galaxies have more gas at 0.1 kpc ∼ 10 kpc. Right panel: the temporal evolution of gas mass within 10 kpc. The dashed line is the median value of 10 Gyr simulation.

obtained the mass flux and velocity of the wind:

$$\dot{M}_{\rm W,H} = \dot{M}_{\rm BH}\left(\frac{r_{\rm tr}}{20\ r_{\rm s}}\right), \tag{5}$$

$$v_{\rm W,H} = 0.2 v_{\rm k}(r_{\rm tr}), \tag{6}$$

where $v_{\rm k}$ is the Keplerian velocity, $r_{\rm s}$ is the Schwarzschild radius and $r_{\rm tr}$ is the truncation radius between the hot accretion flow and truncated thin disk, which is believed to be the standard geometry of the accretion flow when accretion rate is low (Yuan & Narayan 2014). The truncation radius is described by:

$$r_{\rm tr} \approx 3\ r_s \left[\frac{2 \times 10^{-2}\ \dot{M}_{\rm Edd}}{\dot{M}\,(r_{\rm Bondi})}\right]^2, \tag{7}$$

The opening angle of the wind is $\theta \sim 5°$–$50°$ and $130°$–$180°$ above and below the equatorial plane, respectively (Yuan et al. 2015). We do not consider jet in the hot model in the present paper and will consider its effect in future work.

The black hole accretion rate in the hot mode is computed by

$$\dot{M}_{\rm BH,hot} \approx \dot{M}\,(r_{\rm in})\left(\frac{3r_{\rm s}}{r_{\rm tr}}\right)^{0.5} \tag{8}$$

The radiation efficiency as a function of accretion rate is studied in Xie & Yuan (2012), which is

$$\epsilon_{\rm hot}(\dot{M}_{\rm BH}) = \epsilon_0\left(\frac{\dot{M}_{\rm BH}}{0.1\ L_{\rm Edd}/c^2}\right)^a \tag{9}$$

where the values of ϵ_0 and a are given in Xie & Yuan (2012). The Compton temperature used to calculate the radiative heating in the hot mode is (Xie et al. 2017):

$$(T_{\rm C,hot}) = \begin{cases} 10^8, & 10^{-3} \lesssim \dot{M}_{\rm BH}/\dot{M}_{\rm Edd} \lesssim 0.02 \\ 5 \times 10^7, & \dot{M}_{\rm BH}/\dot{M}_{\rm Edd} \lesssim 10^{-3} \end{cases} \tag{10}$$

2.2.2. Star Formation and Stellar Feedback

The star formation is modeled in the same way as in Yuan et al. (2018) but slightly modified in Yao et al. (2021). We implement star formation by subtracting mass, momentum, and energy from the grid. It is triggered only if the temperature is lower than 4×10^4 K and the number density is higher than 1 cm^{-3} concurrently. The star formation rate per unit is given by the Kennicutt-Schmidt prescription:

$$\dot{\rho}_{\rm SF} = \frac{\eta_{\rm SF}\,\rho}{\tau_{\rm SF}} \tag{11}$$

We set the star formation efficiency $\eta_{\rm SF} = 0.01$.

The stellar mass loss rate follows the prescriptions of the stellar evolution theory, with

$$\dot{M}_\star = {\rm IMF}(M_{\rm TO})|\dot{M}_{\rm TO}|\Delta M \tag{12}$$

where the initial mass function (IMF) is a Salpeter law, more details can be seen in Ciotti & Ostriker (2007). The SNe Ia feedback is modeled by injecting pure thermal energy to the ISM. Assuming for each supernova event an energy release of $E_{\rm snia} = 10^{51}$ erg and the time evolution of the SN Ia rate as

$$R_{\rm SN}(t) = 0.32 \times 10^{-12} h^2 \vartheta_{\rm SN}\frac{L_{\rm B}}{L_{\rm B_\odot}}\left(\frac{t}{13.7{\rm Gyr}}\right)^{-s}{\rm yr}^{-1} \tag{13}$$

where the coefficient $\vartheta_{\rm SN} = 1.0$ fixes the present-day SN Ia rate, and $h = 0.6774$, $s = 1.1$. We have also considered stellar physics including Type II supernovae and the stellar wind heating from the old stars (Li et al. 2018). The chemical evolution and dust absorption are ignored for simplicity.

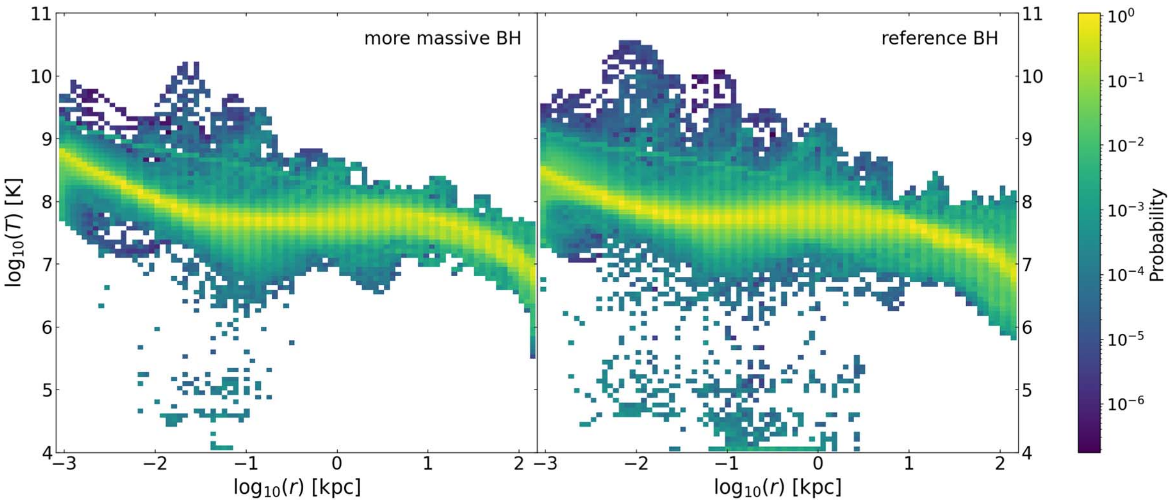

Figure 3. The 10 Gyr stack diagram of temperature vs. radius over the compact galaxy with MAS (left) and REF (right) simulation. Plots are made by stacking the distributions of gas temperature from every simulation output. The color is weighted by the gas mass at this radius, which represents the probability that gas at this radius has this temperature. The REF galaxy shows significantly more scattering in gas temperatures on both the lower ($\lesssim 10^6$ K) and higher ($\gtrsim 10^{10}$ K) temperature ends.

3. Results

3.1. The Evolution of Gas Content

The left panel of Figure 2 shows the gas number density profiles of two compact galaxies averaged over time: one with a more massive black hole (orange) and a reference black hole (blue). The MAS galaxy exhibits lower gas density by a factor of a few at 0.1 kpc $\lesssim r \lesssim$ 10 kpc. However, within 100 pc from the galactic center, the gas density profiles of two galaxies are comparable to the REF galaxy. It suggests that a more massive central BH can efficiently expel the gas at $\sim$10 kpc scale, but the effect is less significant at smaller radii. As will be shown in Section 3.4, this effect is closely related to different AGN feedback strengths of two central BHs.

We further examined the temporal evolution of gas mass within approximately 10 kpc of the compact galaxy in the right panel of Figure 2. Starting from the same gas mass initially, the total gas mass within two galaxies evolves in distinctively different directions. In the REF galaxy, the gas mass remains high ($\sim 9 \times 10^8 M_\odot$) overall time, while in the MAS galaxy, the gas mass experiences a reduction and finally stabilizes at around $3.5 \times 10^8 M_\odot$ in the later stage. This is consistent with the gas density profiles shown in Figure 2. Meanwhile, galaxy gas mass fluctuations are much greater with the reference black hole, which is due to, as will be shown in Section 3.4, more frequent and intense AGN activity.

3.2. Gas Temperature and Cooling

The reduction in gas density with a more massive BH aforementioned has a direct impact on the thermal states and radiative cooling of the gas. In Figure 3, we present stacked diagrams of temperature versus radius over a 10 Gyr period for the compact galaxies with the more massive (left) and reference (right) black hole, where the color bar indicates the gas mass fraction at each radius. Although the temperature distributions of the two galaxies primarily stay at the hot phase and are largely similar, the REF galaxy shows significantly more scattering in gas temperatures on both the lower ($\lesssim 10^6$ K) and higher ($\gtrsim 10^{10}$ K) temperature ends, while the MAS galaxy exhibits a more concentrated temperature distribution. This is consistent with the gas density profiles shown in Figure 2, indicating smooth (chaotic) AGN activities with the more (less) massive central BH. We also note that in both simulated galaxies, little warm/cool gas forming at $r \sim 10^{-2}$–10 kpc can reach the innermost radius of $r \sim 10^{-3}$ kpc, where the gas temperature is always high ($\gtrsim 10^7$ K). We speculate this is because the gas is mixed with/heated to high temperatures by the central AGN and is unable to survive/cool down to lower temperatures.

To examine how the gas temperature change alters gas thermal states, we investigate the cooling time of two galaxies by plotting the difference in $t_{\rm cool}$ radial distribution between two galaxies (galaxy with more massive BH minus the reference one) in Figure 4. Overall, the $t_{\rm cool}$ profiles decrease with smaller radii for both galaxies due to larger gas density in the inner region. However, the $t_{\rm cool}$ distribution of the MAS galaxy is systematically larger than that of the REF galaxy, since as previously mentioned, the gas in the MAS galaxy is of higher temperature and lower density due to the stronger heating and gas expelling by stronger AGN activity. This leads to a longer cooling time in the MAS galaxy rising above the line of $t_{\rm cool}/t_{\rm ff} = 10$, therefore the gas in the MAS galaxy is more

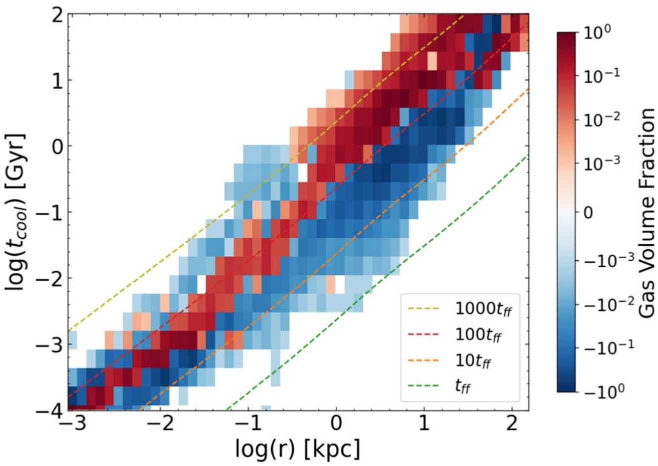

Figure 4. The differences in $t_{\rm cool}$ radial distribution between two galaxies (galaxy with more massive BH minus the reference one). The MAS galaxy has higher gas temperatures and lower densities due to stronger AGN activity, resulting in a systematically larger distribution of $t_{\rm cool}$ compared to the REF galaxy.

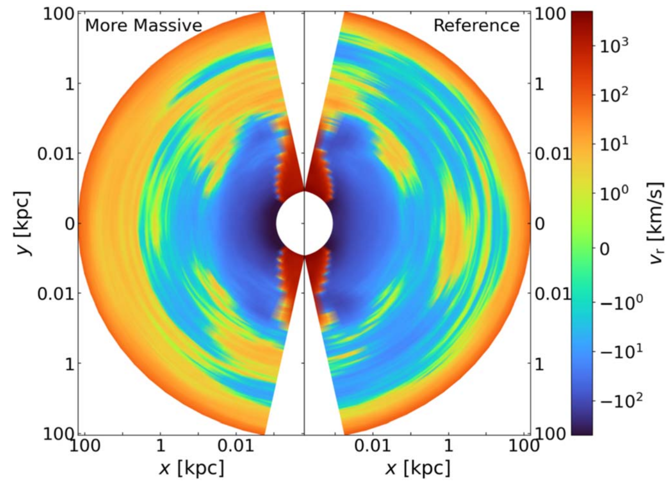

Figure 5. The radial velocity of gas in two compact galaxies. To avoid the effects of strong outflow or inflow, values are used for the median value in 10 Gyr simulation rather than the average value. In the inner regions ($r \lesssim 10$ pc), the AGN wind powers high-radial velocity outflows with $v_{\rm r}$ up to $\sim 10^3$ km s^{-1}.

stable against thermal instability (Sharma et al. 2012; Li & Bryan 2014; Voit et al. 2017). While for the REF galaxy, due to the relatively shorter cooling time, a considerable amount of gas falls below the line of $t_{\rm cool}/t_{\rm ff} \sim 10$ and becomes thermally unstable, leading to the formation of cooler gas which is seen in Figure 3. Magnetic fields might also play a role in stabilizing the gas buoyancy oscillations and enhancing thermal instability (Ji et al. 2018), while we do not include the effect of magnetic fields here and leave this for future work.

3.3. Gas Inflow and Outflow

Figure 5 shows the spatial distributions of gas radial velocity averaged over 10 Gyr in the two compact galaxies. In both simulations, the gas exhibits rich dynamics with inflows and outflows. However, in the inner regions of $r \lesssim 10$ pc where the AGN wind powers high-radial velocity outflows with $v_{\rm r}$ up to $\sim 10^3$ km s^{-1}, the outflows in the MAS galaxy are more spatially extensive than those in the REF galaxy indicating stronger AGN feedback and ability to drive outflows with the more massive BH. This effect also appears at a larger scale of $\sim$0.1 kpc and beyond, where the MAS galaxy produces more extensive outflows than the REF galaxy.

To explore the gas dynamics more quantitatively, we further plot the mass flux of inflows (blue dashed), outflows (red dashed) and net flows (solid) averaged over time of two galaxies in Figure 6. Although the overall trends of inflows and outflows in both galaxies are similar, by examining the net flows, we can find a significant difference in net inflow- and outflow-dominated regions between the two galaxies, where the transition point between the two regions is referred as the "stagnation region". In the MAS galaxy, the stagnation region is located at $\sim$50 pc. In contrast, the stagnation region is located at as large as $\sim$1 kpc in the REF galaxy which is one order of magnitude larger than that in the MAS galaxy. The shift of the stagnation region, as indicated in Figure 5, is due to the stronger AGN feedback in the MAS galaxy. The AGN feedback can drive outflows with higher radial velocities and larger spatial extents, which can reduce the gas fraction in the galaxy and thus reduce the inflow rate.

In addition, we find that both the inflow and outflow rates decrease with decreasing radius in both galaxies. This overall trend of inward decrease is as same as what is found in black hole hot accretion flow (Yuan et al. 2012). We speculate that as in the case of black hole hot accretion flow, it may be due to the presence of convective motion and outflow in the galaxy, as suggested by Yuan et al. (2012). However, the net rate in our simulations is not a constant of radius, which is different from the black hole hot accretion flow in Yuan et al. (2012). This is because we have a gas source from the star, which is not included in the accretion disk-scale study of black hole accretion flow by Yuan et al. (2012). Our result is more similar to the findings of the feeding of the supermassive black hole (SMBH) by stellar winds (Ressler et al. 2018).

In short, a more massive BH in a galaxy can power stronger AGN wind, which can drive outflows with higher radial velocities and larger spatial extents, and thus reduce the gas fraction in the galaxy and reduce the inflow rate. As will be discussed in the following section, the reduction of the inflow rate in turn affects the supply of accreted gas to the black hole.

3.4. AGN Activity and Feedback Strength

In order to understand the activity and impact of the AGN feedback in the simulations, we present the AGN energy output

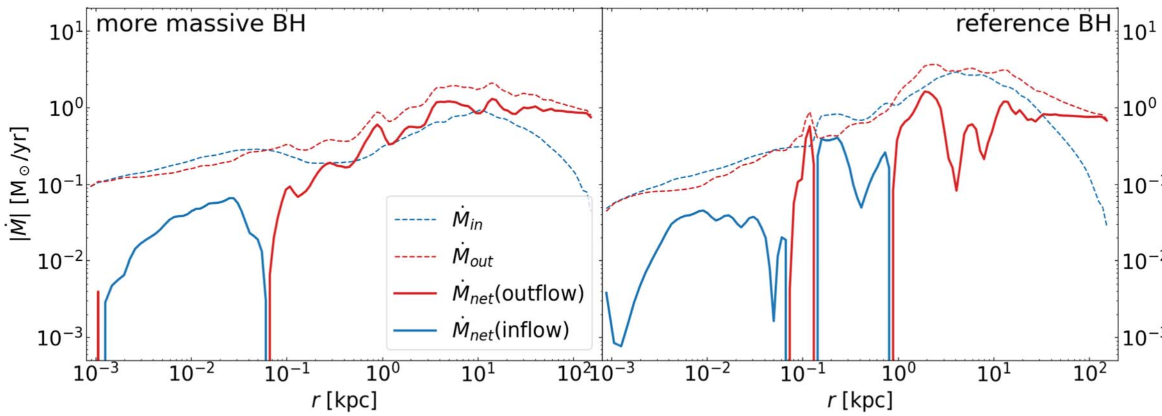

Figure 6. Time averaged and angle averaged accretion inflow rates as a function of the radius in the galaxy with a large black hole. The dotted line is $\dot{M}_{\rm inflow}$(blue) and $\dot{M}_{\rm outflow}$(red). The solid line represents the net flow rate ($|\dot{M}_{\rm inflow} - \dot{M}_{\rm outflow}|$), with blue indicating net inflow and red indicating net outflow. In the MAS galaxy, the stagnation region is located at ∼50 pc. In contrast, the stagnation region is located at as large as ∼1 kpc in the REF galaxy.

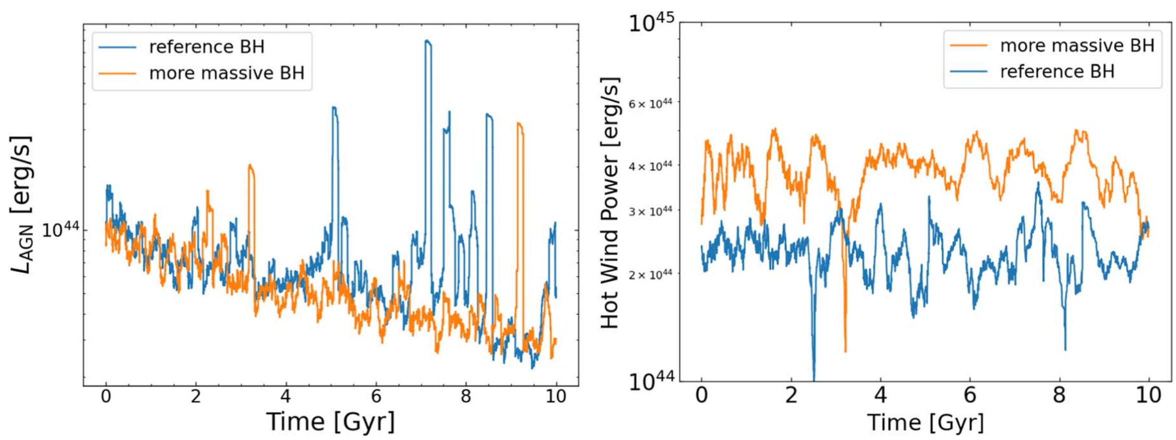

Figure 7. Left panel: light curves of AGN luminosity as a function of time during 10 Gyr. Right panel*:* the AGN wind power with the hot mode, AGN Feedback is in the hot mode most of the simulation time. The AGN evolution is dominated by the hot mode, where the wind power only determined by the accretion rate.

in Figure 7, where the left and right panels show the temporal evolutions of AGN luminosity and wind power, respectively. We find that the AGN luminosities in both galaxies are qualitatively similar, while the one with the reference BH exhibits more frequent outbursts. This is because the reference black hole's small mass makes the gas accretion more likely to reach the critical accretion rate, leading to a higher probability of the AGN feedback mode entering the cold mode, during which the AGN luminosity is higher (Yuan et al. 2018; Yao et al. 2021). But we note that the extra outbursts with radiation feedback do not significantly affect the galactic outflows since we do not include dust, and thus the AGN luminosity is less significant in driving outflows via radiation pressure.

In addition to radiation feedback, the other major feedback mechanism is wind feedback. The AGN wind in the cold mode is related to the luminosity, while the cold mode only occupies an insignificant portion of the total evolution time (less than 0.1% of the 10 Gyr duration). Instead, the AGN evolution is dominated by the hot mode. The right panel of Figure 7 shows that the wind power of the more massive BH is approximately twice as large as that of the reference BH, which demonstrates strong AGN feedback with a more massive BH and is consistent with previous findings (more effective gas expelling, faster outflow velocities, etc.). This is because although the gas supply in the inner regions surrounding two BHs ($r \lesssim 10$ pc) is comparable in mass, the more massive BH can accrete more gas due to its deeper gravitational potential (which is significant at a scale of ∼10 pc), and thus blow out more gas as wind feedback.

3.5. BH Mass Growth

We finally comment on the BH mass growth in the two simulations. The BH mass growth is shown in the third column

Table 1
AGN Activity and Feedback Strength

Simulation	Description of the Central BH	BH Initial Mass ($\times 10^8 M_\odot$)	Stellar Mass ($\times 10^{11} M_\odot$)	BH Mass Growth ($\times 10^8 M_\odot$)	Total Accretion Mass[a] ($\times 10^8 M_\odot$)	Total Wind Mass ($\times 10^8 M_\odot$)	Total Star Formation ($\times 10^7 M_\odot$)	Duty Cycle[b]
MAS	more massive BH	18.0	1.5	1.98	11.5	9.5	0.01	0.04%
REF	reference BH	6.72	1.5	1.53	6.39	4.8	0.48	0.06%

Notes.
[a] The total mass of gas passing through the innermost boundary of simulation.
[b] The fraction of time that galaxy spends above 0.02 $L_{\rm Edd}$.

of Table 1. We find that the more massive BH grows by $1.98 \times 10^8 M_\odot$ which is ∼11% of its initial mass, while the reference BH grows by $1.53 \times 10^8 M_\odot$, ∼24% of its initial mass. The result indicates that it is even harder for a more massive BH to grow in mass. This is because the BH mass growth does not only depend on its initial mass which determines the accretion rate, but also on the outflow rate driven by the AGN feedback. The more massive BH has a higher accretion rate, but also a higher outflow rate due to its stronger feedback strength as shown in previous sections, which leads to a similar BH mass growth as the reference BH. We also test the BH mass growth in a rich-gas environment by carrying out a separate simulation (Di et al. 2023) with a reference mass BH but one-order-of-magnitude greater gas density, while the BH mass only grows by a moderate amount of ∼50% compared to our reference simulation, which is due to the strong AGN feedback which prevents the BH from accreting more gas.

In summary, we find that the growth in the BH mass via gas accretion is very limited, and we thus speculate for isolated galaxies without mergers, it is unlikely that the BH can grow significantly via gas accretion. This indicates that for compact galaxies which bypass the late phase of ex situ star accretion, the central BH must have been massive by the end of the early phase, where the BH mass growth is dominated by cold gas inflows at relatively high redshifts.

4. Conclusion

In this paper, we explore the impact of the SMBH masses on the evolution of compact galaxies, by placing SMBHs of two different masses ($1.8 \times 10^9 M_\odot$ for the more massive BH run MAS and $6.72 \times 10^8 M_\odot$ for the reference run REF) in identical compact galaxy hosts (with a stellar mass of $1.5 \times 10^{11} M_\odot$ and an effective radius of 1.03 kpc) and evolving them over 10 Gyr with star formation and stellar/AGN feedback physics. Our main findings are as follows:

First, a more massive SMBH can expel much more gas from the galaxy, resulting in a lower gas density/fraction with higher temperatures at 0.1 kpc $\lesssim r \lesssim$ 10 kpc. This change in the gas density and temperature significantly increases the cooling timescale in the compact galaxy with the more massive BH, reaching $t_{\rm cool} \gtrsim 100 t_{\rm ff}$ at almost all radii. As a consequence, the gas around the galaxy with a more massive BH is dominated by a single hot phase with a temperature of $T \gtrsim 10^7$ K. In contrast, in the REF simulation with a lower BH mass, the gas at the galaxy scale has a larger density and lower temperatures, resulting in a shorter cooling timescale of $t_{\rm cool} \lesssim 100 t_{\rm ff}$, even $\lesssim 10 t_{\rm ff}$ in some regions which are thus subject to thermal instability, and the gas tends to be multiphase with a significant amount of cool/warm gas of 10^4 K–10^6 K.

In addition to the gas thermal state, the gas kinematics is also distinctively different in the two simulations. At small scales of $\lesssim$10 pc where the outflows are determined by AGN feedback physics, the MAS simulation produces more spatially extensive outflows with velocity up to a few 10^3 km s^{-1} due to the larger BH mass. At galactic scales of ∼100 pc–1 kpc, the MAS simulation also exhibits more prominent outflows with a velocity of ∼100 km s^{-1}, with the stagnation point (which is the location where the net flow is zero) located at ∼0.1 kpc, much smaller than that in the REF simulation (which is at ∼1 kpc). The gas kinematics is consistent with the picture that gas is more effectively expelled in the MAS simulation.

With further investigation, we conclude that the difference in gas thermal states and kinematics can be explained by the interplay between gas properties and AGN activities, which leads to different AGN feedback strengths. We find that the AGN hot wind in the MAS simulation is twice as powerful as that in the REF simulation due to the larger BH mass in MAS and comparable gas supply immediately around BHs in both simulations. The more powerful AGN wind in the MAS simulation can more effectively expel gas from the galaxy, resulting in a lower gas density/fraction and higher temperature at 0.1 kpc $\lesssim r \lesssim$ 10 kpc, and thus a longer cooling timescale. In contrast, the AGN wind in the REF simulation is less powerful, and the gas density/fraction and temperature are higher, resulting in a shorter cooling timescale and single-phase gas. We also note that compared with MAS, the AGN in REF is more likely to be in the cold mode due to its smaller BH mass (and thus a lower critical accretion rate for the transition from cold to hot mode), and exhibits more frequent outbursts. However, since dust is not included in our simulations, the impact of AGN radiation pressure on the gas during the cold mode might be underestimated. We hope to improve this in future work.

We finally examined the BH mass growth and find that the BHs only grow moderately within an order of magnitude in both simulations, and the more massive BH in MAS even grows by a lower percentage of its initial mass ($\sim$11%) than the one in REF ($\sim$24%) over the 10 Gyr duration. This is because of the overdominant impact of AGN feedback which is highly effective in expelling surrounding gas, reducing the accretion rate and impeding the growth of the central BHs. The AGN feedback is even more significant in the MAS run with a more massive BH. Therefore, we speculate that the over-massive SMBHs in compact galaxies detected in the observations, without experiencing any merging event, cannot grow themselves efficiently via gas accretion, and thus are more likely formed by the end of the early phase of galaxy formation at relatively high redshifts of $z \gtrsim 2$.

Acknowledgments

We would like to thank the referee for providing a constructive report which improves this paper, and Yuan Li for helpful discussions. YD, FY, and SJ are supported by the National Natural Science Foundation of China (grants 12133008, 12192220, and 12192223). The calculations have made use of the High Performance Computing Resource in the Core Facility for Advanced Research Computing at the Shanghai Astronomical Observatory.

ORCID iDs

Yihuan Di https://orcid.org/0000-0003-1717-6697

References

Ciotti, L., & Ostriker, J. P. 2007, ApJ, 665, 1038
Daddi, E., Renzini, A., Pirzkal, N., et al. 2005, ApJ, 626, 680
de la Rosa, I. G., La Barbera, F., Ferreras, I., et al. 2016, MNRAS, 457, 1916
Dehnen, W. 1993, MNRAS, 265, 250
Di, Y., Li, Y., Yuan, F., Shi, F., & Caradonna, M. 2023, MNRAS, 523, 1641
Ferré-Mateu, A., Mezcua, M., Trujillo, I., Balcells, M., & van den Bosch, R. C. E. 2015, ApJ, 808, 79
Ferré-Mateu, A., Trujillo, I., Martín-Navarro, I., et al. 2017, MNRAS, 467, 1929
Gaspari, M., McDonald, M., Hamer, S. L., et al. 2018, ApJ, 854, 167
Gaspari, M., Ruszkowski, M., & Oh, S. P. 2013, MNRAS, 432, 3401
Gofford, J., Reeves, J. N., McLaughlin, D. E., et al. 2015, MNRAS, 451, 4169
Graham, A. W., Durré, M., Savorgnan, G. A. D., et al. 2016, ApJ, 819, 43
Hayes, J. C., Norman, M. L., Fiedler, R. A., et al. 2006, ApJS, 165, 188
Hopkins, P. F., Bundy, K., Murray, N., et al. 2009, MNRAS, 398, 898
Ji, S., Oh, S. P., & McCourt, M. 2018, MNRAS, 476, 852
Li, Y., & Bryan, G. L. 2014, ApJ, 789, 153
Li, Y.-P., Yuan, F., Mo, H., et al. 2018, ApJ, 866, 70
Naab, T., Johansson, P. H., & Ostriker, J. P. 2009, ApJL, 699, L178
Navarro, J. F., Frenk, C. S., & White, S. D. M. 1996, ApJ, 462, 563
Oser, L., Ostriker, J. P., Naab, T., Johansson, P. H., & Burkert, A. 2010, ApJ, 725, 2312
Quilis, V., & Trujillo, I. 2013, ApJ, 773, L8
Ressler, S. M., Quataert, E., & Stone, J. M. 2018, MNRAS, 478, 3544
Sazonov, S. Y., Ostriker, J. P., Ciotti, L., & Sunyaev, R. A. 2005, MNRAS, 358, 168
Sazonov, S. Y., Ostriker, J. P., & Sunyaev, R. A. 2004, MNRAS, 347, 144
Shakura, N. I., & Sunyaev, R. A. 1973, A&A, 24, 337
Sharma, P., McCourt, M., Quataert, E., & Parrish, I. J. 2012, MNRAS, 420, 3174
Shi, F., Li, Z., Yuan, F., & Zhu, B. 2021, NatAs, 5, 928
Szomoru, D., Franx, M., & van Dokkum, P. G. 2012, ApJ, 749, 121
Trujillo, I., Conselice, C. J., Bundy, K., et al. 2007, MNRAS, 382, 109
Trujillo, I., Ferré-Mateu, A., Balcells, M., Vazdekis, A., & Sánchez-Blázquez, P. 2013, ApJ, 780, L20
Trujillo, I., Schreiber, N. M. F., Rudnick, G., et al. 2006, ApJ, 650, 18
van den Bosch, R. C. E., Gebhardt, K., Gültekin, K., et al. 2012, Natur, 491, 729
van Dokkum, P. G., Nelson, E. J., Franx, M., et al. 2015, ApJ, 813, 23
van Dokkum, P. G., Whitaker, K. E., Brammer, G., et al. 2010, ApJ, 709, 1018
Voit, G. M., Meece, G., Li, Y., et al. 2017, ApJ, 845, 80
Walsh, J. L., van den Bosch, R. C. E., Gebhardt, K., et al. 2016, ApJ, 817, 2
Werner, N., Lakhchaura, K., Canning, R. E. A., Gaspari, M., & Simionescu, A. 2018, MNRAS, 477, 3886
Xie, F.-G., & Yuan, F. 2012, ApJ, 427, 1580
Xie, F.-G., Yuan, F., & Ho, L. C. 2017, ApJ, 844, 42
Yang, H., Yuan, F., Yuan, Y.-F., & White, C. J. 2021, ApJ, 914, 131
Yao, Z., Yuan, F., & Ostriker, J. P. 2021, MNRAS, 501, 398
Yuan, F., Bu, D., & Wu, M. 2012, ApJ, 761, 130
Yuan, F., Gan, Z., Narayan, R., et al. 2015, ApJ, 804, 101
Yuan, F., & Narayan, R. 2014, ARA&A, 52, 529
Yuan, F., Wu, M., & Bu, D. 2012, ApJ, 761, 129
Yuan, F., Yoon, D., Li, Y.-P., et al. 2018, ApJ, 857, 121